Tellus (1985), *37A*, 209–232

Fractal properties of rain, and a fractal model

By S. LOVEJOY, *EERM/CRMD, Météorologie Nationale, 2 Avenue Rapp, 75007 Paris, France* (now at *Physics Department, McGill University, Montreal H3A 2K6, Canada*) and B. B. MANDELBROT, *IBM T. J. Watson Research Center, Yorktown Heights, New York 10598, USA* (also at *Mathematics Department, Harvard University, Cambridge MA 02138, USA*)

(Manuscript received March 20; in final form November 26, 1984)

ABSTRACT

This paper amplifies upon earlier theories and observations by the authors, advances a probabilistic model of rain fields, and exhibits realistic simulations, which the reader is advised to scan before continuing with the text. The model is also compared with other approaches. The theory of fractals has been in part motivated by the Hurst effect, which is an empirical observation in hydrology and climatology. A fractal is an unsmooth shape that is scaling, that is, where shape appears unchanged when examined by varying magnifications. The study of fractals is characterized by the prevalence of hyperbolically distributed random variables, for which $\Pr(U > u) \propto u^{-\alpha}$, where Pr is the probability that the value of the variable exceeds u, and α is a positive exponent. Lovejoy established the applicability of fractals in meteorology, by showing that cloud and rain areas project on the Earth along shapes whose boundaries are fractal curves, and that the temporal and spatial structure of rain is rife with hyperbolically distributed features. These observations, as amplified in this paper, set up the challenge of constructing fractal models with the observed properties. The models presented here belong to a very versatile family of random processes devised in Mandelbrot: fractal sums of (simple) pulses, or FSP processes. The simulations to be presented reveal that these processes involve a scaling heirarchy of "bands", "fronts", and "clusters", as well as other complex shapes, none of which had been deliberately incorporated in the process. This very rich morphology and the related statistical distributions exemplify the power of simple fractal models to generate complex structures, and are in accord with the wide diversity of actual rainfall shapes. It is argued that this model already provides a useful context in which the basic statistical properties of the rainfield, including the relationship between the temporal and spatial structure, may be studied.

1. Introduction

A striking feature of rainfall is its extreme spatial and temporal variability. Over a wide range of time and space scales, sudden changes occur so frequently that rainfall is often intuitively described as "erratic". In fluid mechanics, the analogous phenomenon of abrupt transitions is called "intermittency", which is the terminology we use here. Mandelbrot's systematic studies of intermittency have revealed its profound links with scaling and with hyperbolic distributions.

A phenomenon is called scaling when it involves no characteristic scale of length or time. In particular (Mandelbrot and Van Ness, 1968), a random function $X(t)$ is called scaling at the origin, if $X(0) = 0$ and $X(\lambda t) \stackrel{d}{=} \lambda^H X(t)$ for all ratios $\lambda > 0$. Here $\stackrel{d}{=}$ denotes identity in statistical distribution and H is a scaling exponent.

More generally, $X(t)$ is scaling for all times if, for arbitrary t_0 and t_1, the symbolic relation $\Delta X(\lambda \Delta t) \stackrel{d}{=} \lambda^H \Delta X(\Delta t)$ holds between the quantities $\Delta t = t_1 - t_0$, $\Delta X = X(t_1) - X(t_0)$, $t_2 = t_0 + \lambda(t_1 - t_0)$ and $\Delta X(\lambda \Delta t) = X(t_2) - X(t_0)$. When λ is large, this is a relation between large-scale variation over the long time lag $\lambda \Delta t$, and small scale variation over the short time lag Δt. The notation $\Delta t, \Delta X$ is meant to emphasize that scaling refers to *differences*. The graphs of scaling functions, and other related geometric shapes are "fractal sets" (Mandelbrot 1975, 1977, 1982) characterized by a "fractal dimension" that is a non-integer quantity related to H.

A random variable U is called hyperbolic if the

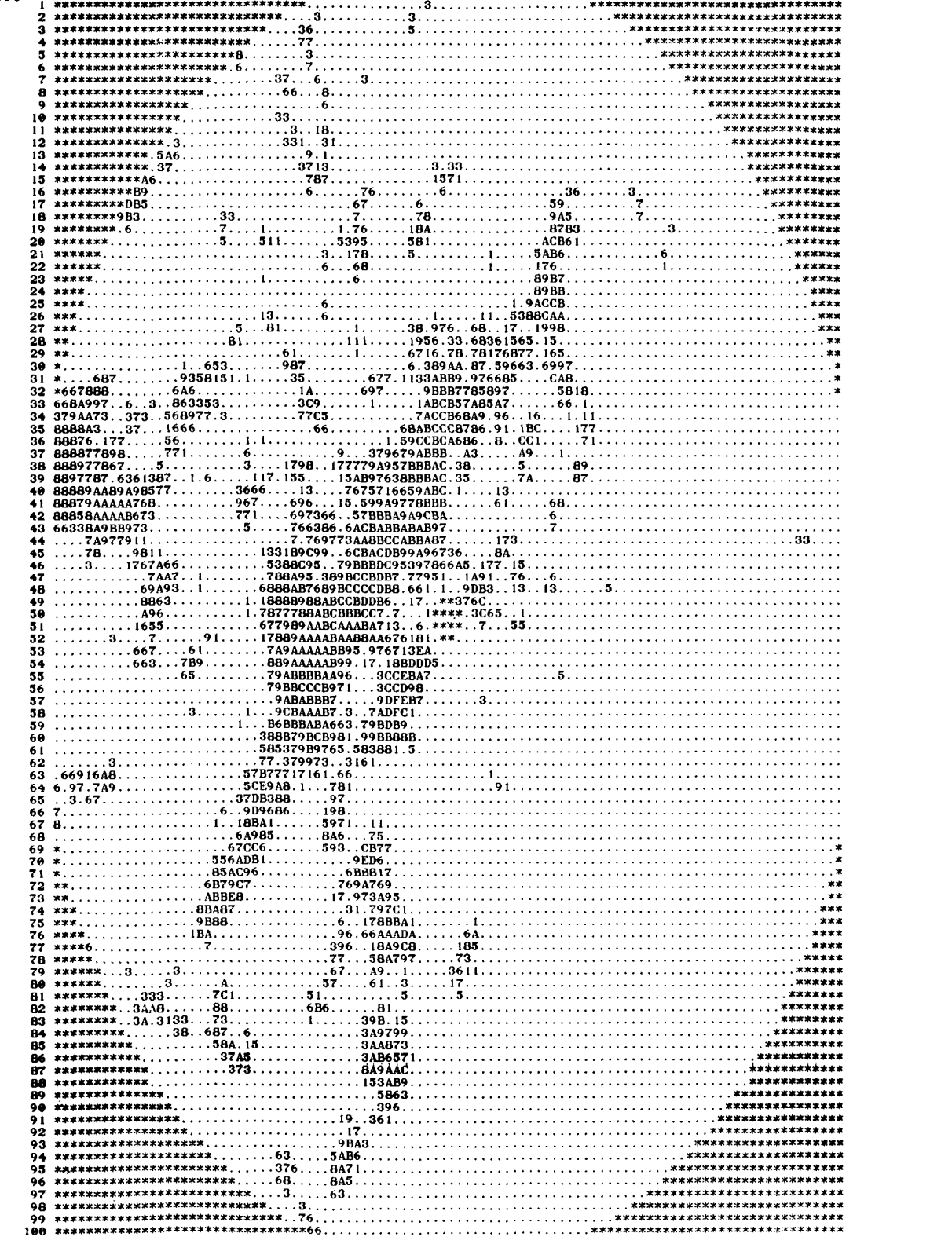

tail probability $\Pr(U > u)$ takes the form $\Pr(U > u) \propto u^{-\alpha}$. (The custom is to denote a random variable by a capital letter, and its value by the corresponding lower case letter.) Mandelbrot (1974, 1984a) showed that a broad family of intermittent fluctuations, now called "multiplicative chaos", leads to such a distribution for the intermittent quantity. On the rôle of hyperbolic distributions in meteorology, see also Schertzer and Lovejoy (1984b).

The smaller the value of α, the larger are the extreme values of U; in fact, the moment (U^h) is finite for $h < \alpha$ but diverges for $h \geqslant \alpha$. This last property requires comment. Since sample moments are always finite, divergent theoretical moments used to be viewed as strange and abnormal, and as sufficient to make hyperbolic random variables "improper" for modeling nature. In fact, a divergent theoretical moment merely expresses that the sample moment does not converge to any limit and can become arbitrarily large. Mandelbrot (1963a, b) was the first to show that such is indeed the case in important natural fluctuations: not only do hyperbolic random variables fit a broad variety of data, but samples constructed with such variables turn out to contain a variety of "configurations" that often seem so clear-cut as to make it difficult after the fact to believe that they are due to "mere chance". On a broader scene (Mandelbrot, 1975, 1977, 1982), very simple fractal mechanisms prove to have the ability to generate seemingly complex samples. In any event, the hyperbolic distribution's properties differ sharply from those of the customary Gaussian distribution and from those of its elementary transforms such as the lognormal distribution.

Lovejoy tested the applicability of scaling, fractals and of the hyperbolic distributions to the study of the rainfield. In particular, Lovejoy (1982) established the absence of fundamental length scales and hence the fractal nature of the perimeters of rain and cloud fields (at least from 1 km^2 to 1.2 $\times$ 10^6 km^2), and Lovejoy (1981) established the existence of hyperbolic fluctuations in rain rate from many areas of the world. One purpose of this paper is to record these experimental results in more complete and more accessible form.

This paper's second purpose is to construct a stochastic fractal model which produces scaling and hyperbolically intermittent fields. This new family of fractals, introduced in Mandelbrot (1984b), involves fractal sums of simple pulses. The specific model used here involves only 3 parameters and seems rather structureless. Yet a glance at the simulations reported later in this paper shows that they are true to what one should expect of fractals, and reproduce many of the characteristics known (Fig. 1) to be present in rainfields: (i) scaling, (ii) intermittency, (iii) complexity of forms, (iv) the hierarchy of line-like structures, (v) the distribution of rain areas, (vi) clustering of "cells" at all scales.

Section 2 examines the empirical evidence for the scaling and hyperbolic intermittency. Section 3 decribes a scaling stochastic model. Section 4 fits this model to various rainfall statistics. Section 5 compares this scaling model to earlier models based upon specified hierarchies and discusses some general arguments in favor of scaling and of fractals. Finally, Section 6 is devoted to conclusions.

2. Empirical evidence for scaling and hyperbolic intermittency in the rain field

2.1. *Evidence for hyperbolic temporal intermittency*

It is natural to observe the fluctuations in the flux of rain from an isolated rain area. This was done with radar data in Montreal, Spain and the tropical Atlantic with 4 $\times$ 4 km spatial, and 5 min temporal resolution. By their nature, rain areas frequently split apart or merge together; it is therefore necessary to establish a criterion for their definition and selection.

In a first study, reported in Fig. 2a, b, c, Lovejoy picked those areas that had maintained their identity for at least 100 min, with only minor splits. Rain areas were followed until a major split or merger occurred, after which the area was considered "dead" (see Tsonis and Austin (1981) for details). Less than 10% of all areas satisfied these criteria. Minor splitting is allowed, but

Fig. 1. Radar rain map at 3 km altitude taken by H.M.S. *Quadra* in the tropical Atlantic. Symbols, first in numerical and then in alphabetic order, indicate rain rates on a log scale, 8 symbols per decade in rain rate. Resolution is 4 $\times$ 4 km. Asterisks indicate sea clutter noise (center only), and the maximum radar range (220 km). Note the prevalence of straight lines, commonly referred to as "bands" or "fronts".

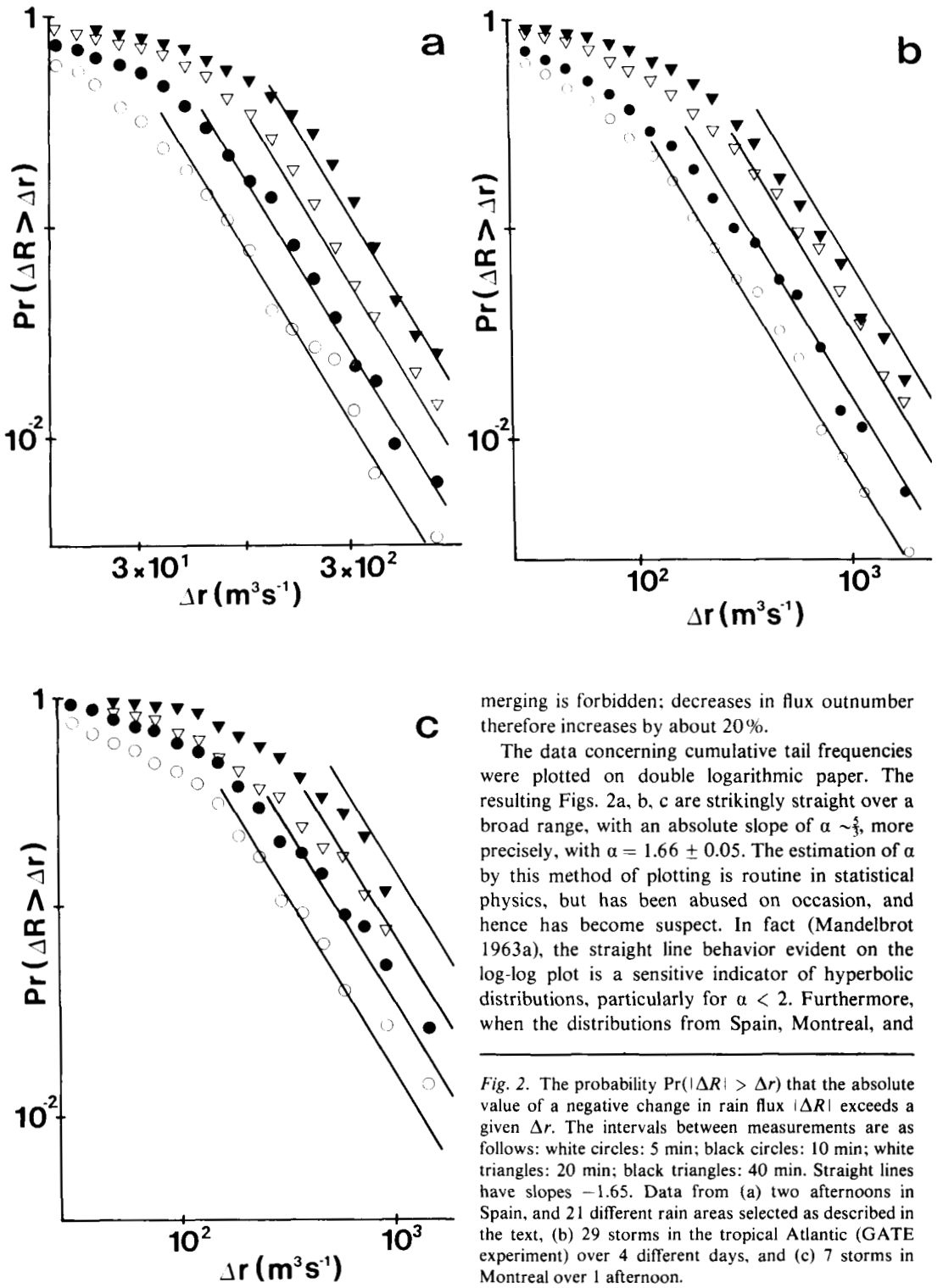

merging is forbidden; decreases in flux outnumber therefore increases by about 20%.

The data concerning cumulative tail frequencies were plotted on double logarithmic paper. The resulting Figs. 2a, b, c are strikingly straight over a broad range, with an absolute slope of $\alpha \sim \frac{5}{3}$, more precisely, with $\alpha = 1.66 \pm 0.05$. The estimation of α by this method of plotting is routine in statistical physics, but has been abused on occasion, and hence has become suspect. In fact (Mandelbrot 1963a), the straight line behavior evident on the log-log plot is a sensitive indicator of hyperbolic distributions, particularly for $\alpha < 2$. Furthermore, when the distributions from Spain, Montreal, and

Fig. 2. The probability $Pr(|\Delta R| > \Delta r)$ that the absolute value of a negative change in rain flux $|\Delta R|$ exceeds a given Δr. The intervals between measurements are as follows: white circles: 5 min; black circles: 10 min; white triangles: 20 min; black triangles: 40 min. Straight lines have slopes -1.65. Data from (a) two afternoons in Spain, and 21 different rain areas selected as described in the text, (b) 29 storms in the tropical Atlantic (GATE experiment) over 4 different days, and (c) 7 storms in Montreal over 1 afternoon.

the tropical Atlantic are normalized so as to yield the same mean flux, the distributions of ΔR cannot be statistically distinguished by Komolgorov–Smirnov tests. If the positive and negative Δr's are normalized separately, they are also distributed similarly.

Additional support for hyperbolic behavior with $\alpha \sim \frac{5}{3}$ comes from Fig. 3, where a different rain area selection criterion was used. All areas that neither split nor merged on two consecutive scans were used—about 50% of the areas present. During the 3 h during which data were collected, the total flux of all storms increased by 40%. However, positive and negative Δr's were almost equal in number (238 and 213 respectively). Most of the increase is therefore due to the fact that in absolute value, the large positive Δr's exceed by ~50% the large negative Δr's (Fig. 3). Subintervals exhibiting R and decreasing flux yielded similar distributions, except that the relative magnitude of the distributions of large positive and large negative Δr's was different. In all cases, the $(\Delta r)^{-1.65}$ asymptotic behavior was unaffected.

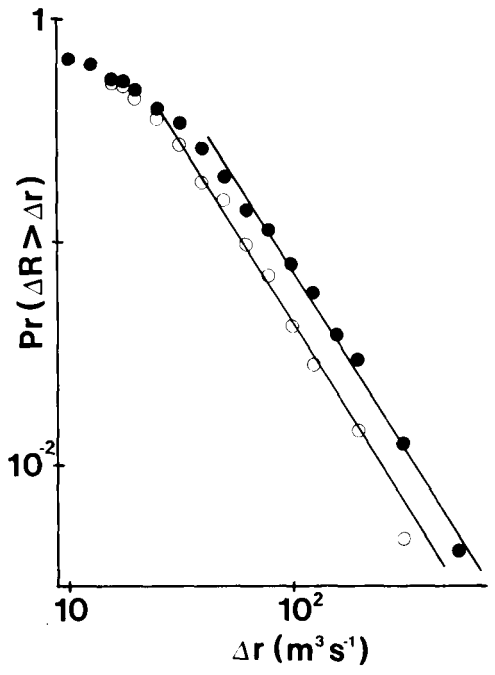

Fig. 3. The probability $\Pr(|\Delta R| > \Delta r)$ of the absolute change in rain flux over 5 min, $|\Delta R|$ exceeding a fixed Δr; positive changes, black circles; negative changes, white circles. Data are from the tropical Atlantic; rain areas were selected as described in the text.

It should be noted that these results are unlikely to be artifacts of the radar data processing. Indeed (Mandelbrot, 1963a), the hyperbolic tail of the distribution is in general insensitive to the presence of both additive and multiplicative types of noise. In the case of rainfall, these may be the radar reflectivity fluctuations due to incoherent scattering. (The only exception, which is not of concern here, is when the noise is itself hyperbolic with a lower α value). This insensitivity is supported by the agreement found here in the value of α for different radars in different parts of the world.

2.2. *Evidence for temporal scaling*

If we write the distributions shown in Fig. 2 as:

$$\Pr(\Delta R > \Delta r) \sim (\Delta r/\Delta^* r)^{-\alpha},$$

the quantity $\Delta^* r$ measures the "width" or amplitude of the ΔR. If the rainfield is scaling in time, then $\Delta^* r \propto (\Delta t)^{H_L}$ (naturally, the coefficient of proportionality depends on the units of r and t). The subscript "L" is used here to indicate that H_L is a "Lagrangian" parameter, relative to fluctuations following the flow. Doubling Δt implies (as observed in Fig. 2), that the "width" increases by the constant distance H_L log 2 on a log-log plot. The parameter H_L was estimated in two ways. (A) Sampling the intercurve distance in Fig. 2 four times every decade (starting for $\Pr < 0.1$) yielded $H_L = 0.69 \pm 0.06$. (B) The best straight-line asymptote was fitted on the assumption that $\alpha = \frac{5}{3}$, thus determining $\Delta^* r(\Delta t)$, and H_L was determined by a regression of log $(\Delta^* r)$ against log Δt. This yielded $H_L = 0.59$. We conclude that $H_L = 0.64 \pm 0.05$.

In nature, scaling rules tend to hold over a finite scale range between a positive "inner cutoff" and a finite "outer cutoff". The value of the outer cutoff is a very important characteristic of a problem. Very long time scales, which are usually associated with the climate, have been studied by Hurst (1951), who discovered a remarkable empirical rule that applies for example to river discharges and rain data (as well as to other geophysical variables). Mandelbrot (1965) argued that the puzzling "Hurst phenomenon" should be viewed as a symptom of scaling. Mandelbrot and Wallis (1968, 1969) broadened the scope of this explanation. Very short time scales, which are usually associated with turbulence, are also known to be scaling down to a

very short inner cutoff ruled by viscosity. A coherent picture of the entire spectrum from seconds to hundreds of thousands of years (similar to the study of temperature in Lovejoy and Schertzer (1983), see Subsection 4.4) would be illuminating.

2.3. *Evidence for horizontal scaling*

Using individual radar maps, we may evaluate $\Pr(\Delta R > \Delta r)$ for different spatial separations Δx. Two examples taken from GATE data are shown in Fig. 4. Note that they only differ in the width $\Delta^* r$. This was also found to be true in all other cases analyzed, namely in a total of 23 randomly chosen radar PPI's. From the separation between the curves, we estimate that $H_E \sim 0.50$. The subscript "E" is used here to indicate that H_E is relative to a "Eulerian" reference frame-fixed relative to the flow. When using radar data to evaluate these distributions, care must be taken not to introduce any range-dependent radar data processing effects. Here, ΔR was determined cross-range in a narrow band, so as to compare equal-sized sampling volumes.

Note that in the diagram in Fig. 4, the asymptote is curved, meaning that the distribution is *not* hyperbolic, contrary to Figs. 2 and 3. We think this feature is associated with a certain degree of spatial smoothing of the extreme rainfall gradients. This effect is relatively easy to model and is discussed in Section 3. We note that the mean square (ΔR^2) is finite when taken in space, while it is infinite when taken in time because $\alpha \sim \frac{5}{3}$.

It is possible to estimate H_E by a statistical method called R/S analysis. The letters R/S denote a quantity called "rescaled range", which was originally introduced by Hurst (1951) and subsequently used by Mandelbrot and Wallis (1969) and Mandelbrot (1972) as the basis of a new procedure for studying long-run dependence in empirical time series. This statistic is robust, in the sense that its behavior is only influenced by long-run dependence, and is insensitive to large fluctuations around the long-term trend. R/S analysis has the disadvantage that it is biased for short series of

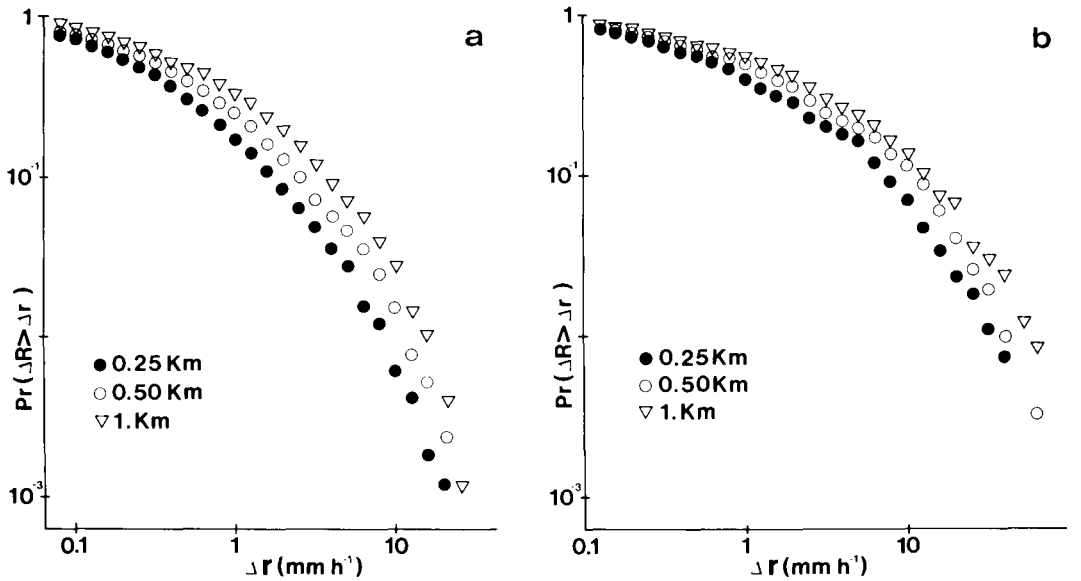

Fig. 4. The distribution $\Pr(\Delta R > \Delta r)$ of the rain rate gradient, ΔR for gradients over 0.25, 0.5, 1.0 km distances. (a) is from a single radar map and (b) shows the distributions for the 24 different randomly chosen radar scans studied, which differed only in their "width" (amplitude) and not in their shape or scaling. Data are from the tropical Atlantic GATE experiment, Canadian ship *Quadra*. Gradients were measured cross-range so as to avoid range-dependent radar-measurement biases. As the separation is doubled, the distributions are multiplied by the factor 2^{H_1} with $H_E \sim 0.50$.

data. We applied it separately for data at ranges of 50, 100, 150 km from the radar. Applying R/S analysis cross-range for separations of 20° to 50° (radar resolution of 1°) showed that $H_E = 0.48 \pm 0.02$ for 5 km $< \Delta X <$ 13 km, 10 km $< \Delta X <$ 26 km, 15 km $< \Delta X <$ 39 km.

Either the probability distribution method or R/S analysis may be used to estimate H_E, but both are limited in the scales over which they may exhibit scaling because of the limited range of radar data, and because of the necessity of avoiding range-dependent biasing effects with the radar.

The true limit of horizontal scaling is a basic meteorological problem, since all meteorological fields are strongly interrelated and the existence of a length scale in one may be expected to be reflected in the others. Furthermore, in the last 10 years, many experiments have attempted to detect length scales—particularly in the velocity field. These experiments have found no clear evidence of any basic length scale between the turbulence dissipation scale, of the order of centimeters, and planetary scales. Readers are referred to Schertzer and Lovejoy (1984a, b) for a reivew of the relevant empirical and theoretical arguments in favor of the scaling hypothesis.

Direct support for the scaling of the rain and cloud fields is found in Lovejoy (1982). Here, the fractal relation between the area A and the perimeter P, as derived in Mandelbrot (1977, 1982), is used to show that $P \propto \sqrt{A}^D$ with $D \sim 1.35$, for rain and cloud areas between 1 km^2 and 1.2×10^6 km^2. The coefficient of proportionality necessarily depends on the unit of length. This result has recently been extended down to 2.6×10^{-2} km^2 with LANDSAT imagery (private communication, Cahalan et al. (1984). The exponent D is the fractal dimension of the perimeter and is a measure of the perimeter's "complexity". Smooth perimeters are well-known to satisfy $P \propto \sqrt{A}$; hence $D \sim 1$, and maximally complicated perimeters that literally fill the plane satisfy $P \propto A$, and hence $D \sim 2$. The fact that no deviations from $D \sim 1.35$ are found for lengths in the region from 0.16 km to 1000 km is direct evidence for scaling.

It would have been tempting to use the fractal area–perimeter relation to estimate H_E, since Mandelbrot (1977, 1982) shows that Gaussian fluctuations satisfy $H + D = 2$. However, the empirical value of this sum is $H_E + D \sim 1.85 < 2$. This discrepancy is not completely understood, but may indicate that the rain field is definitely non-Gaussian.

3. Description of the fractal rain model

3.1 Mandelbrot's stable-Levy model of the Noah effect, and storm time series

Before turning to our one-, two- and three-dimensional FSP models, it is instructive to translate in terms of rainfall time series a very simple model that has proven useful in economics and elsewhere (Mandelbrot 1963b, 1982). This model is not applicable to rain areas, but it already demonstrates the basic features of intermittency exploited in the more realistic FSP models. Fig. 5 shows the result of adding independent identically distributed hyperbolic random variables with $\alpha \sim \frac{5}{3}$; the number of variables added is labeled as time and varies from 1 to 1300. Positive and negative increments were chosen with equal probability, and the sum is interpreted as a model of the time series of total rain flux from an isolated storm. For $\alpha < 2$, a generalized central limit theorem (see e.g. Feller (1971)) shows that the sum of independent identically distributed hyperbolic random variables converges to a stable-Lévy variable. This limit's probability density is complicated, being only asymptotically hyperbolic, but with the same exponent α. Therefore, if the rule $\Pr(\Delta R > \Delta r) \propto (\Delta r)^{-\alpha}$ is extended down to $\Delta r \to 0$, the result is

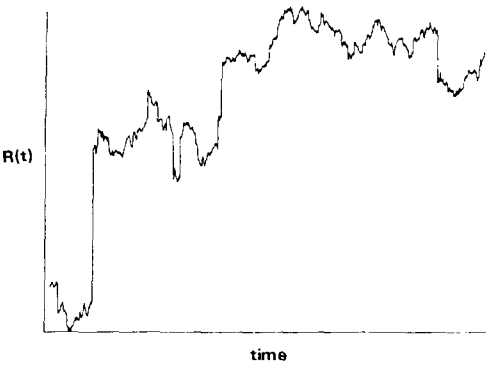

Fig. 5. Monte-Carlo simulation of a rainfall time series $R(t)$ constructed by adding 1300 consecutive independent random variables from the distribution $(\Delta r)^{-5/3}$. Positive and negative changes were equally likely. Note that in any interval, most of the change in $R(t)$ is due to one large "jump", hence the term "erratic".

scaling. In particular, independent increments yield $H = 1/\alpha \sim \frac{3}{5} = 0.60$. This model therefore has stable-Levy increments. Fig. 5 is drawn with values of α and H close to those of actual rainfall data analyzed in Figs. 2 and 3. Since successive fluctuations are independent in Fig. 5, the best prediction concerning future values of $R(t)$ is that there will be no persistence, that is, no change on the average. This conclusion agrees with the results of Tsonis and Austin (1981) and Tsonis et al. (1984), but may not hold for all processes with similar α and H. It would be interesting to examine the question of predictability in the model presented below.

Fig. 5 illustrates a basic property of random functions whose increments are hyperbolically distributed with $\alpha < 2$. *A priori*, these increments are identically distributed. *A posteriori*, however, the largest increment is most unusual: it is of the same order as the sum of all the others, and thus dominates this sum. In Fig. 5, this effect may be seen by inspecting any interval: a large fraction of the total change in $R(t)$ comes from a single large "jump". Mandelbrot and Wallis (1968) called this feature the "Noah effect" after the extreme 40 day, 40 night fluctuation responsible for the biblical flood. The fact that a single large fluctuation may dominate the others is quite different from the situation made familiar by the Gaussian or quasi-Gaussian cases, where individual fluctuations rarely exceed several standard deviations, and even the largest fluctuation is negligible compared to the sum—this being a criterion for the sum's convergence to the Gaussian. We show below that the counterparts of this fact in more refined models permit a much greater richness in structure, including a scaling hierarchy of clusters and line-like shapes.

3.2. *Mandelbrot's fractal sums of pulses (FSP) in one dimension*

Consider (Fig. 6) a function $R(t)$ that is the sum of rectangular pulses of random heights, representing a rainfall intensity increment ΔR, random widths, representing the rainfall duration ρ, and random centers, distributed according to a Poisson process with a constant rate ν. In the framework of the usual stochastic models, one assumes (without even saying so) that the expectations relative to the pulses, $\langle \rho \rangle$ and $\langle \Delta R \rangle$, are both finite and are taken to constitute two

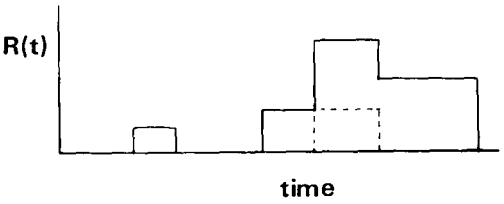

Fig. 6. Schematic view of the "rectangular pulse" rain model showing three elementary "pulses". The process used in the text results when the duration and intensity are related in the manner described in the text, and the duration is distributed as ρ^{-1}.

characteristic scales. An implementation of these assumptions is found in Rodriguez-Iturbe (1983). Under these assumptions, however, the sum of the pulses is a strongly scale-dependent process, whose properties for $T \gg \langle \rho \rangle$ are completely different from its properties for $T \ll \langle \rho \rangle$.

Mandelbrot (1984c) advances several ways of insuring that the sum is scaling. The simplest is to choose $\Pr(\rho' > \rho) \propto \rho^{-1}$ as the probability of a random duration ρ' exceeding ρ and to let $\Delta R = \pm \rho'^{1/\alpha}$. This means that, for a given duration ρ', the pulse intensity ΔR is of fixed absolute value and of random sign. (Here, the letter ρ' is used to denote the random variable whose values are ρ, because the Greek "capital rho" is identical to P.) Note that this model makes the radical assumption that $\langle \rho \rangle = \infty$; this is necessary in order for the sum to be scaling. In one dimension, Mandelbrot (1984b) refers to this simplest rectangular pulse as a "cancelling echo", since the initial impulse ΔR is "echoed" at a distance ρ' by an equal and opposite "cancelling" impulse.

This model is scaling, with the exponent $H = 1/\alpha$, because increasing length scales by the factor λ only changes the intensity of the echoes by the factor $\lambda^{1/\alpha}$. This may be understood by noting that the number of echoes over an interval of length l, whose length exceeds ρ, is $l\Pr(\rho' > \rho) = l\rho^{-1}$, and hence is invariant under the scale transformations $l \to \lambda l$, $\rho \to \lambda \rho$. By construction, the increments of the process are hyperbolic of exponent α.

As to the increment over the interval l, it is the sum of hyperbolic increments and its tail distribution is hyperbolic. However, it does *not* follow a stable-Levy distribution. The distribution it follows is a new one introduced in Mandelbrot (1984b), for which the condition $\alpha < 2$ is not necessary. The

discrepancies are very interesting, but they are minor for $\alpha \sim \frac{5}{3}$, and need not concern us here.

The scaling argument (although not the hyperbolicity argument) also works when the pulses are no longer rectangular, but smooth or continuous, as long as their length scales as λ and their intensity as $\lambda^{1/\alpha}$. A convenient pulse shape used in later sections is $\Delta R \exp\{-[u/\rho]^{2s}\}$, where u is the distance from the center of the echo. This shape is somewhat arbitrary, but is convenient: by varying s, the echo can be made as smooth or as discontinuous as desired. In the limit $s \to \infty$, the pulses are rectangular.

It is important to note that, although smoothing doesn't affect the scaling, it does considerably alter the probability distributions of the (Eulerian) gradients. Only in the case of sharply rectangular pulses ($s = \infty$) does one obtain hyperbolic gradients ($\alpha_E = \alpha$). In the smooth echo case, the Eulerian gradients are rarely large (rapid fall-off in the probability distributions). Fortunately, as we show below, the Lagrangian gradients remain hyperbolic, $\alpha_L = \alpha$.

Mandelbrot (1984b) also studies more general FSP processes, and other "cancelling echo" processes, and derives expressions for their characteristic functions, showing in particular that increments of the above process are hyperbolic, with α as parameter for all $\alpha < 2$. He also studies a model in which ΔR and ρ' are chosen independently, allowing $H < 1/\alpha$.

3.3. *Computer simulations of the FSP process in one dimension*

The implementation is straightforward. We seek a simulation whose minimum resolution ρ_i (the "inner scale") is taken as 1 pixel, and whose "outer scale" is ρ_0. We model this process by placing pulse centers uniformly at random over the interval $(0, L)$, v per unit length, with pulse lengths distributed as $\Pr(\rho' > \rho) = \rho^{-1}$ for $\rho > 1$. The amplitudes are simply $\Delta R = \pm \rho'^{1/\alpha}$. Such samples exhibit "edge" effects due to the fact that the probability of finding a large jump is smaller near the edges than in the center, because large jumps' centers are far away. However, the sample's center of length $l \ll L$ will be scaling, with the parameter $H = 1/\alpha$ up to the outer scale $\rho_0 = vL$ (because on average, this will be the longest pulse). In practice, $L/l = 6$ was usually used although $L/l \sim 3$ would probably suffice. Fig. 7 shows an example of the FSP process with 50,000 pulses, $\alpha = \frac{5}{3}$.

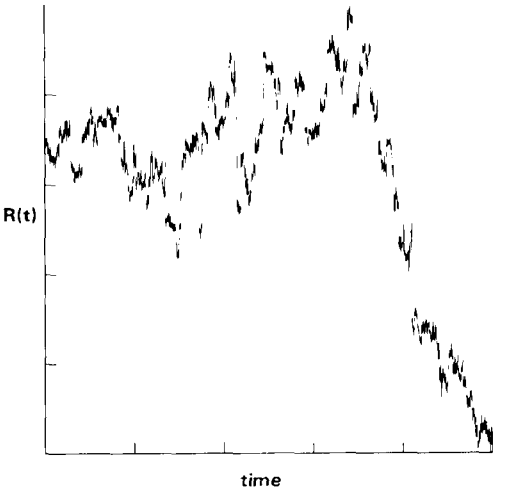

Fig. 7. The FSP process $R(t)$ produced with $l = 10{,}000$, $L = 20{,}000$, $v = 2.5$, $\alpha = \frac{5}{3}$, $(H = \frac{3}{5})$, $\rho_i = 1$, $\rho_0 = 50{,}000$.

3.4. *Two-dimensional FSP processes*

We encounter a considerably richer structure in the x,y plane than in the linear cross sections described above. In this case, the horizontal cross section can take any desired shape. In the following, we only treat the isotropic case, and we follow closely the procedures that Mandelbrot (1984b) derived from the very different problem of the texture of the distribution of galaxies studied in Chapter 35 of Mandelbrot (1982).

In 2-D, the simplest pulse is a straight cylinder whose base is a circle. In this case, the distribution of the pulse areas should be $\Pr(A > a) = a^{-1}$, for $a > 1$. Furthermore, $\Delta R = \pm A^{1/\alpha}$. It is not hard to show that random 1-D sections will be FSP processes with pulse lengths distributed as ρ^{-1}, as before. The centers of the circles are now placed uniformly at random in a square $L \times L$ and only the central part $l \times l$ (with $l \ll L$ as before) is used. The result is shown in Fig. 8a.

The field $R(x, y)$ cannot be immediately interpreted in terms of a rain rate because the value of $R(x, y)$ is almost surely negative at some points. In practice, a threshold R_T is set, the rain rate is measured as the difference $R - R_T$, and negative values are reset to zero like in the fractal mountain of Mandelbrot (1982). The model rain rate is then

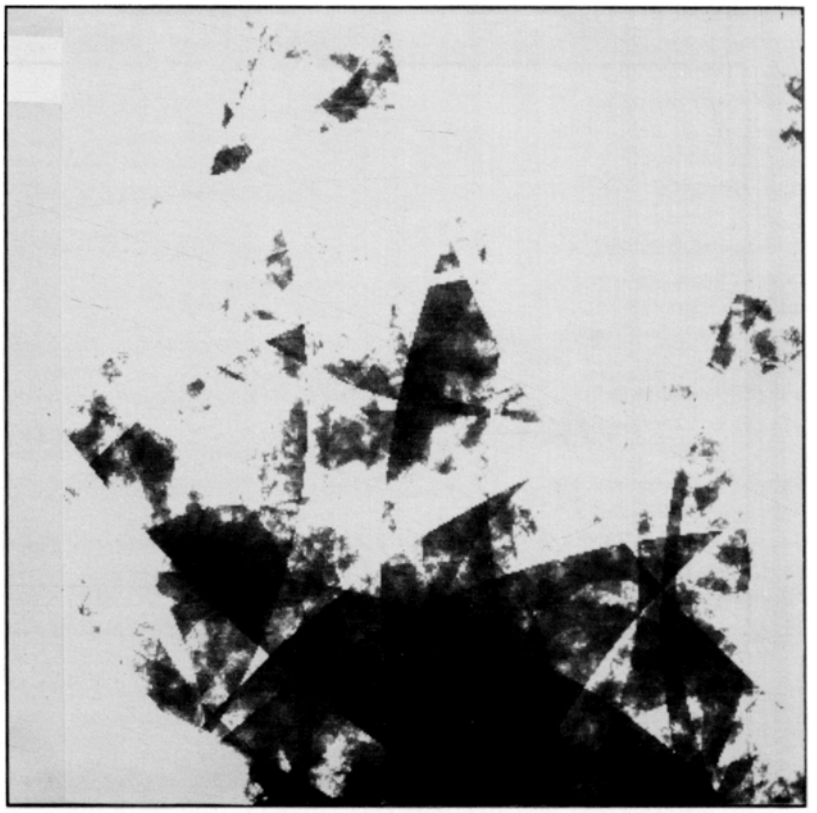

Fig. 8. The pulse process in 2-D on a 400 × 400 grid; 160,000 echoes are used, the smallest value of the radius ρ is 3 units. Going down to circles $\rho = 1$ requires significantly more computer time but barely changes the result. This simulation corresponds to $v = 0.025$, $\rho_0 = 1200$ and $L/l = 6$. Here, $s = \infty$ was used (a sharp echo edge) which accounts for the clearly visible circle edges. The log rain-rate is on a grey scale, and R_T was determined such that 30% of the simulation is "raining". Using $s = 8$, the discontinuous sharp "edges" would disappear.

$R' = R - R_T$ for $R > R_T$, and $R' = 0$ for $R < R_T$. Finally, in order to accommodate the large range of rain rates, and to simulate a radar PPI scope, the log of the resulting field is displayed on a grey scale. In practice, it was convenient to determine R_T by the condition that rain covers a given fraction of the area; it is usually taken, somewhat arbitrarily, as equal to 30%.

From Fig. 8a, it is obvious that the R-x and R-y cross sections of the pulse are too sharply discontinuous—they correspond to the 1-D case shown in Fig. 7. Such pulse edges are far too clearly visible to be realistic. As in the 1-D case, we may alleviate this difficulty by using a continuous pulse, in this case $\Delta R \exp[-(u/\rho)^{2s}]$ for circles of radius ρ with u the distance from the circle center. When $s = 8$, we obtain the much more realistic looking simulation, shown in Fig. 8b. However, the probability distributions are no longer hyperbolic—Fig. 9.

Note that in Fig. 9, the rectangular ($s = \infty$) case shows a hyperbolic regime ($\alpha = \frac{5}{3}$) as expected, but that a rapid fall-off occurs at very large Δr. This behavior is entirely due to thresholding. If R_T is set sufficiently low such that 100% of the model area is covered by rain, no truncation occurs, and the probability distribution is $(\Delta r)^{-\alpha}$, as expected. Qualitatively, this may be understood as a consequence of the Noah effect.

Also evident in Fig. 9 is the fact that for the smooth pulse with $s = 8$, the distributions' fall-off is far more rapid in the model than in the data. This

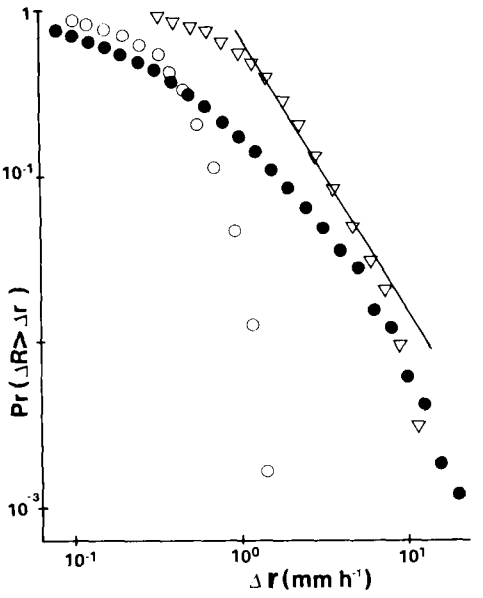

Fig. 9. The distribution of model rain-rate gradients $\Pr(\Delta R > \Delta r)$. The discontinuous ($s = \infty$) case in Fig. 7a is shown as triangles, the continuous ($s = 8$) case in Fig. 7b is represented by open circles, and the data for 0.25 km (from Fig. 4a) is shown by closed circles. The model curves are in arbitrary units and have been separated by half an order of magnitude for clarity of presentation. The straight line indicates a function of the form $(\Delta r)^{-5/3}$. The $s = \infty$ curve deviates from this at large Δr because the thresholding of low rain rates systematically truncates the very large Δr values.

defect must be corrected in future more realistic models, possibly by relaxing the condition of rigid dependence between ρ' and ΔR.

The "circular base" model has at least two defects. First, the number of separate rain areas is too small to be realistic: it tends to produce one or two very large areas and few small ones. Using a notion introduced in Chapter 34 of Mandelbrot (1982), this model is called "excessively lacunar". It is desirable to introduce a new procedure with a new parameter to control the lacunarity by breaking all the areas into smaller ones. A second defect is that, although the model can produce line-like structures (the edges of enormous circles), and thus model rain "fronts", it does not in general produce the bands that are also characteristic of real rain shapes. The simplest method of eliminating both defects is to choose a different pulse basis: to replace the circles by annuli of equivalent area with pulses having a smooth cross section as in Fig 8b (see Fig. 10 for an intermediate stage of construction of an annulus model).

If we take a unit annulus with an outer radius of Λ, area π, then

$$(\Lambda^2 - \Lambda^{*2}) = 1, \qquad \text{hence} \qquad \Lambda^* - \sqrt{\Lambda^2 - 1}.$$

Furthermore, the mean radius δ and the annulus width σ satisfy

$$\delta = \tfrac{1}{2}(\Lambda^* + \Lambda), \qquad \sigma = \tfrac{1}{2}(\Lambda - \Lambda^*).$$

Increasing Λ causes the annuli to become thinner ($\delta \to 0$). The areas of annuli are chosen as before, with $\Pr(A > a) \propto a^{-1}$. Fig. 11 shows the effect of varying Λ (white on black background to simulate the appearance of clouds). As Λ increases from $\Lambda = 1$ (circles) to $\Lambda = 1.4$ (thin annuli), the large structures become increasingly fragmented and banded and other new structures appear. Large rain-free regions (lacunas) become rare, and the number of small rain areas increases. The value $\Lambda = 1.2$ yields fairly realistic looking fields. Fig. 12 shows an example (white on black background to simulate the appearance of clouds) showing the effect of varying ν, α for $\Lambda = 1.2$. Note the appearance of bands and other line-like structures. To facilitate computation, the pulse shape used here is $\Delta R \exp\{-[(u^2/\rho'^2) - \delta^2]/\sigma^2\}^{2s}$, which yields a smooth annulus of "size" ρ'.

As a final example of what can be achieved by varying the basic pulse shape, the circles can be replaced by ellipses with varying eccentricities. Fig. 13 shows a case with high eccentricity. As with the circular base model, the ellipses can be made into elliptical annuli. Fig. 14 shows the effect of increasing the analogous elliptical lacunarity from $\Lambda = 1$ to $\Lambda = 1.25$.

3.5. Three-dimensional FSP processes used to simulate temporal evolution

We have shown how to use a FSP process with continuous pulses to simulate the 2-D rain field, including the gradient probability distributions (with $H_E = 0.60$ instead of the measured value of 0.50). We how show that this model also reproduces the basic hyperbolic distribution of fluctuations in total rain flux from isolated storms. In order to proceed, we clearly need to produce a time series of 2-D rain fields. The simplest way to do this is to assume that the time coordinate has the same properties as the x, y coordinates. This

Fig. 10. An intermediate stage of construction of an annulus model with $\nu = 0.06$, $s = 12$, $\Lambda = 1$, $\rho_0 = 2400$, drawn on an 800 × 800 grid. If ν is increased to $\nu \sim 0.25$ as in Fig. 9, the annuli are no longer visible.

assumption is the Taylor hypothesis of "frozen" turbulence. The exact limits of its validity in the atmosphere are not clear, but Zawadzki (1973) has verified it directly from at least 5 to 40 min with radar rain data, and Brown and Robinson (1979) have shown that it holds up to at least 1000 km for wind fluctuations. This large range of applicability of this hypothesis is directly related to the fact that for atmospheric dynamics, the Kolmogorov $-\frac{5}{3}$ power law spectrum probably holds out to thousands of kilometers in the horizontal, and up to at least 50 h in time (Larsen et al., 1982). Therefore, over this range at least, the first-order statistics of temporal and spectral correlations are the same. In any case, the comparison of a model based on this hypothesis with actual rain data should be illuminating.

Fig. 15 shows a time series made by generalizing the 2-D annular pulses into 3-D spherical shells in the space of coordinates x, y and t, and then making a series of cross-sectional cuts at different values of t. Here the volume V must have the

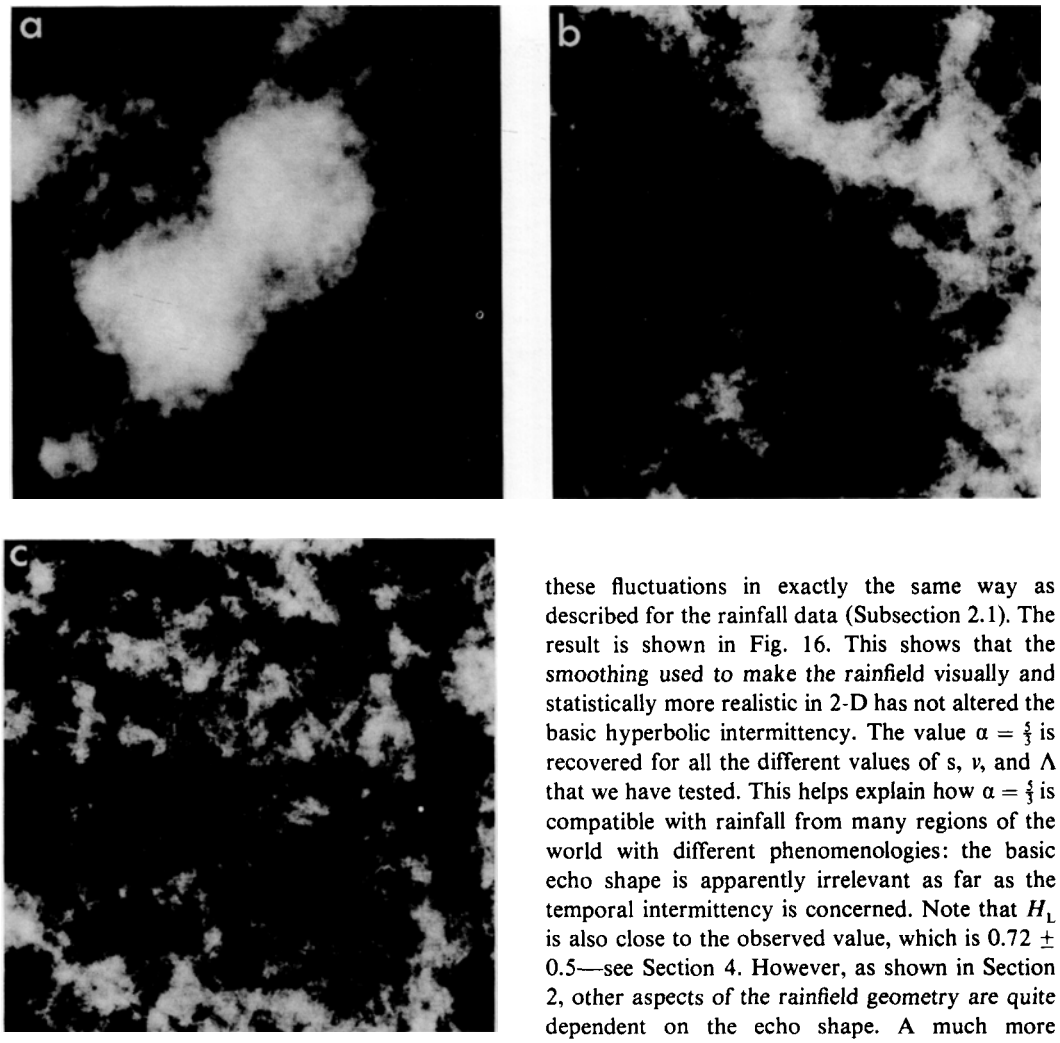

Fig. 11. The effect of changing Λ on a 400 × 400 grid. Here, the log rain intensity is shown as a "white" scale on a black background. The resemblance to cloud shapes is not accidental, since cloud shapes are similar to rain shapes in several ways (see Lovejoy (1982), Lovejoy et al. (1983) for some empirical comparisons). In these illustrations, $s = 4$, $L/l = 3$, $\rho_0 = 1200$, $v = 10$, and $\Lambda = 1$; (a), $\Lambda = 1.2$; (b), $\Lambda = 1.7$ (c).

distribution $\Pr(V > v) \propto v^{-1}$ and $\Delta R = \pm V^{1/\alpha}$. Note that in this model, as in real rainfall, the largest rain areas have, (i) the longest characteristic time, and, (ii) the largest mean rain rate.

To verify that fluctuations from the fractal storms have hyperbolic fluctuations, we evaluated these fluctuations in exactly the same way as described for the rainfall data (Subsection 2.1). The result is shown in Fig. 16. This shows that the smoothing used to make the rainfield visually and statistically more realistic in 2-D has not altered the basic hyperbolic intermittency. The value $\alpha = \frac{5}{3}$ is recovered for all the different values of s, v, and Λ that we have tested. This helps explain how $\alpha = \frac{5}{3}$ is compatible with rainfall from many regions of the world with different phenomenologies: the basic echo shape is apparently irrelevant as far as the temporal intermittency is concerned. Note that H_L is also close to the observed value, which is 0.72 ± 0.5—see Section 4. However, as shown in Section 2, other aspects of the rainfield geometry are quite dependent on the echo shape. A much more exhaustive study of rainfield geometry is obviously necessary to determine which shapes are the most realistic under different meteorological conditions.

4. Further aspects of fractal meteorology

4.1. The fractal dimension of FSP rainfall perimeters

To see whether or not the shapes are as complex in the model as in real rain, it is of interest to determine the fractal dimension D of the model's rain perimeters. The theoretical determination of this D is related to the notoriously difficult "zero-crossing" problems of probability theory. Under certain conditions (e.g. see Mandelbrot

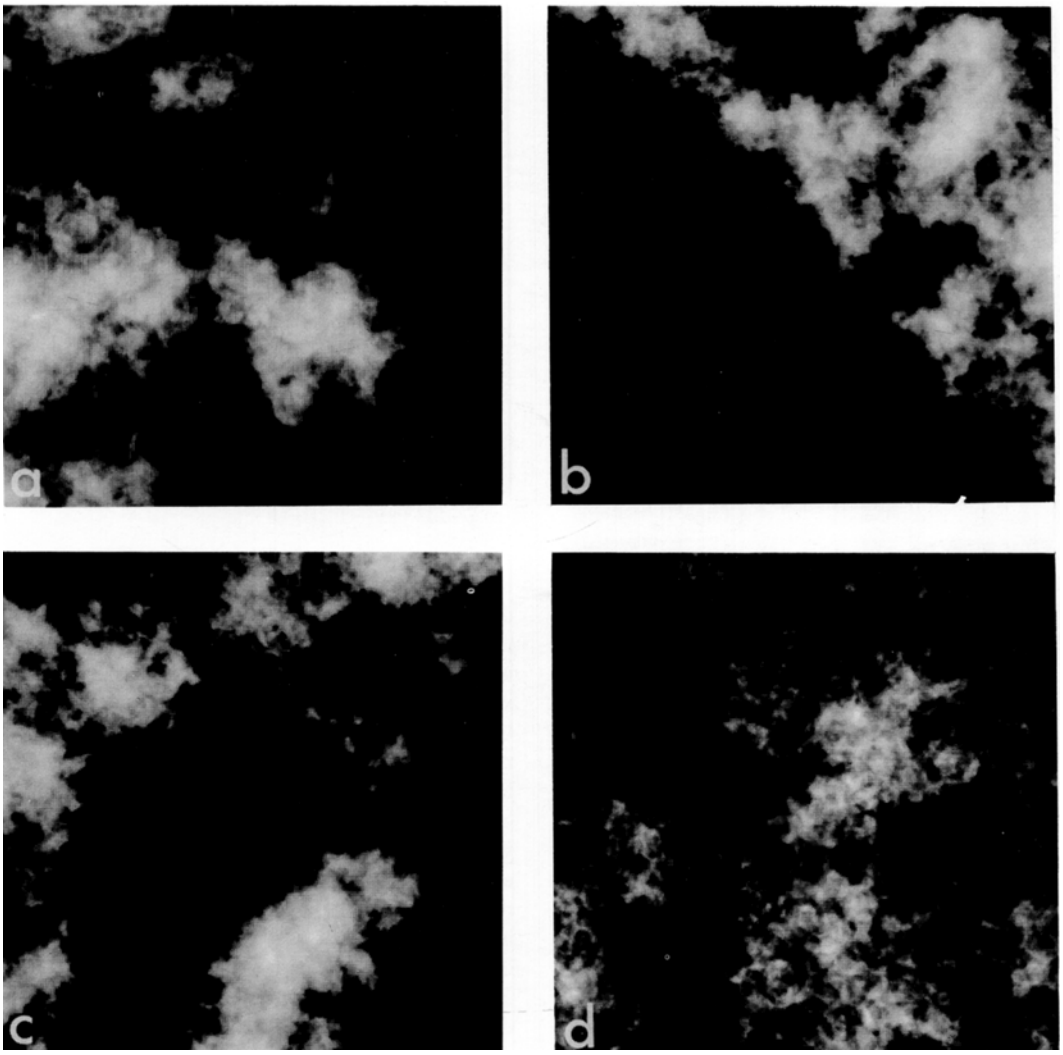

Fig. 12. The effect of changing ν and α on a 300 × 300 grid. The first two model parameters are $s = 2$, $\rho_0 = 900$, $\Lambda = 1.2$, and the other parameters are as follows: (a) $\alpha = \frac{5}{3}$, $\nu = 0.25$; (b) $\alpha = \frac{5}{3}$, $\nu = 1$; (c) $\alpha = \frac{5}{3}$; $\nu = 2.5$; (d) $\alpha = 5$, $\nu = 0.25$.

(1982)), one finds that $H + D = 2$. Although we advocate caution in applying this rule, we have numerically confirmed that it holds for FSP processes. Thus, for $\alpha = \frac{5}{3}$ and $H = \frac{3}{5}$, it predicts $D = \frac{7}{5} = 1.40$. Hetschel and Procaccia (1984) have used $H + D = 2$ to estimate the dimension of cloud perimeters as $D = 1.38$.

4.2. *The distribution of FSP rain areas*

A general property of fractal fields (Mandelbrot, 1977, 1982) is that $\Pr(A > a) \propto a^{-B}$ for the distribution of the areas a bounded by fractal curves, with a positive parameter B. Any other form of the probability distribution would involve the introduction of a length scale and would break the scaling. In the quasi-Gaussian case (e.g. for islands in the ocean) one finds theoretically that $B = \frac{1}{2}D$. Here, we did not attempt to derive the value of B theoretically but evaluated it numerically, obtaining $B = 0.5 \pm 0.5$. This value is somewhat lower than that found empirically: Fig. 17 shows rain area distributions obtained from near instan-

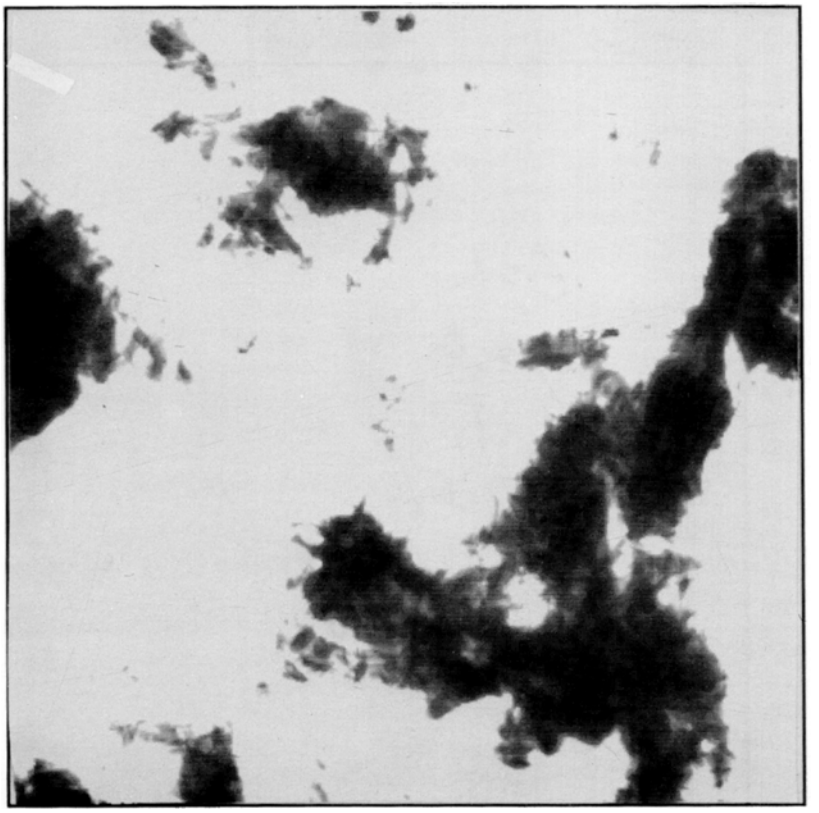

Fig. 13. A series showing the elliptical model on a 400 × 400 grid, $\alpha = \frac{5}{3}$, $s = 2$, $\nu = 0.25$, $\Lambda = 1$, $\rho_0 = 1200$, and a high average eccentricity. Fig. 14a shows an intermediate case in the same series.

taneous radar pictures showing $B \sim 0.75$. More realistic models, with lower values of H_E, to be studied elsewhere, may lead to an increase in B.

The area distribution provides a convenient way to study the interaction of space and time scales—in particular, the effect of "pooling" rain areas over many consecutive radar maps—as is usually the practice when calculating empirical rain area distributions (e.g. Lopez, 1977). In the model, the effect of pooling data from consecutive x, y slices is relatively easy to understand because of the complete equivalence of space and time (1 model unit of time = 1 model unit of space). Pooling simulated areas over model time T clearly introduces a length scale $L = T$.

Fig. 18 shows the effect of pooling rain areas from a 120 × 120 simulation every $\Delta T = 4$ time units for a total of 80 units (i.e. $N = 20$ consecutive 2-D simulations). The $a^{-0.5}$ behavior extends to areas of ~200 (pixel)^2 after which a rapid fall-off occurs. Simulations show that the exact point of transition depends on ΔT, N as well as the initial conditions, for example, the fraction of area covered by rain at the beginning of the sequence, and even on the initial random "seed". Extremely long sample time series are necessary to remove this pooling effect. In real data, the situation is complicated because the space–time relationship is undoubtedly less simple than in the model, and the space/time conversion factor is not known and may vary. The empirical distributions almost always involve pooling to increase the data base; hence their interpretation, is not straightforward. Also shown in Fig. 16 is the empirical GATE distribution replotted from Houze and Cheng (1977) obtained from one scan per day over the entire 90 day GATE experiment. Note that the $a^{-0.75}$ behavior extends out to $a \sim 10^4$ km^2. The

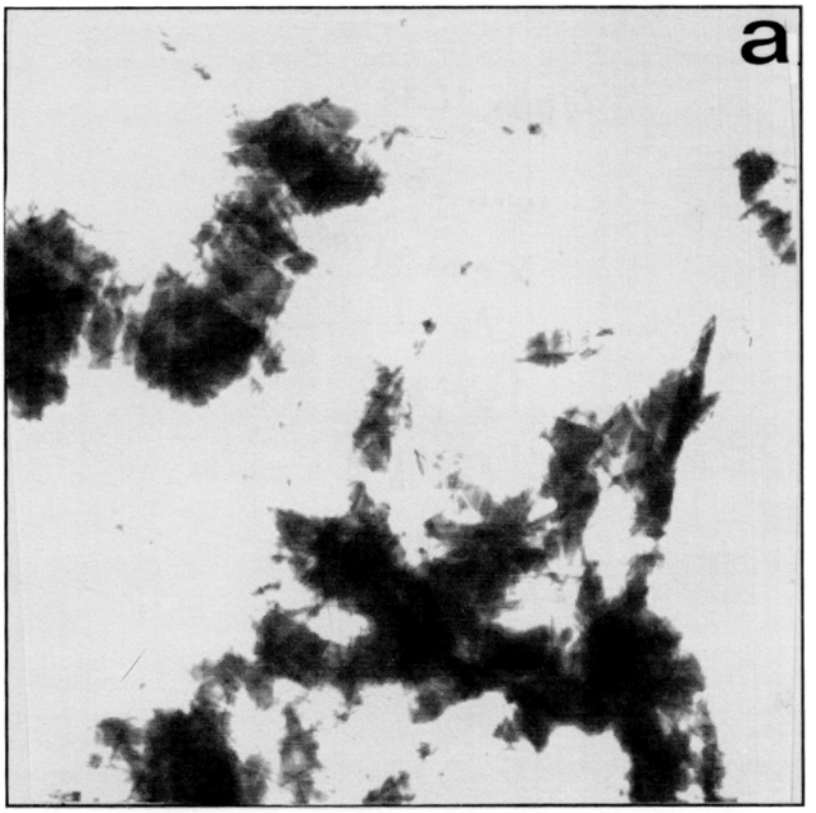

Fig. 14a.
Fig. 14. A series showing the effect of changing the lacunarity parameter Λ from $\Lambda = 1$ (a) to $\Lambda = 1.2$ (b), on a 400 × 400 grid; $\nu = 0.25$, $s = 2$, $\rho_0 = 1200$.

truncation for a larger probability indicates that the sampling was over an insufficiently long time period, although the limited area of reliable radar coverage (~50,000 km^2) could also account for the observed fall-off.

4.3. *The elliptical dimension of atmospheric motions*

At small scales, atmospheric motions appear three-dimensional and at large scales they appear two-dimensional. It has often been conjectured that a "dimensional transition" separates the small and large scale motions. However, Schertzer and Lovejoy (1984a, b) propose a model in which the atmosphere is neither two- nor three-dimensional, in scaling, but anisotropic.

In this model, the horizontal motions are governed primarily by energy transfer, yielding $H = \frac{1}{3}$ in the horizontal, and the vertical motions primarily by the buoyancy force variance transfer, yielding $H = \frac{3}{5}$ in the vertical. These very different scaling exponents lead to the phenomenon of "stochastic stratification", i.e., to fields that appear increasingly stratified at larger and larger scales according to a well-defined scaling mechanism characterized by an "elliptical dimension" (Schertzer and Lovejoy (1985)) $D_{el} = 2 + (\frac{1}{3})/(\frac{3}{5}) = \frac{23}{9} = 2.555 \ldots$ Using this effective dimension to express anisotropy yields plausible vertical cross sections of rain fields (see, Schertzer and Lovejoy (1984a)).

4.4. *The transition from meteorology to climatology*

Lovejoy and Schertzer (1983, 1984) examine temperature and paleotemperature series and find (ignoring the diurnal cycle and its harmonics) that local temperatures are scaling up to periods of ~1 month (the "synoptic maximum"), after which they become stationary. The average hemispheric tem-

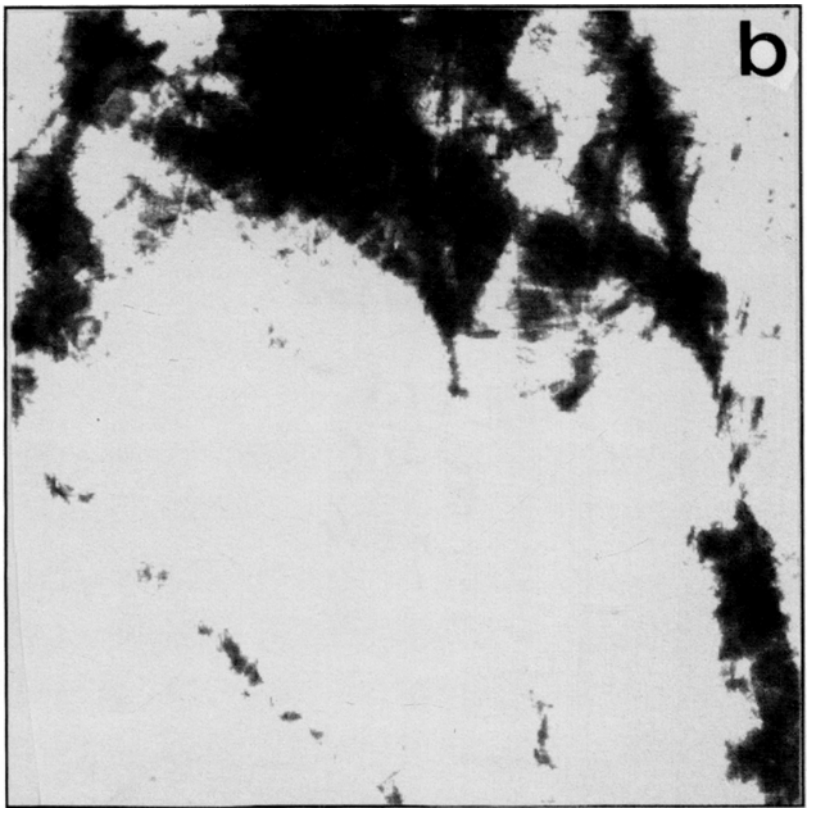

Fig. 14b.

peratures also appear to be scaling from ~40,000 years down to at least 5 years with almost exactly the same value of H (~0.4). To model this behavior, the authors assume that the fundamental differences between meteorological and climatological temperatures are the length and time scales over which they are averaged. They speculate that the break in the scaling for local temperatures at ~1 month would disappear in true globally-averaged temperatures. Although these results are preliminary, it would be interesting to determine whether averaging over larger and larger areas affects the spectrum of rainfall fluctuations in the same way.

5. Discussion. Comparison of the fractal models, including FSP, with earlier models of rainfall

The literature contains a variety of stochastic models of rainfall based upon the assumption that not only the physics but also the geometry of rainfall take different forms over different scale ranges. For reviews of this general approach, see especially Waymire and Gupta (1981), Rodriguez-Iturbe et al. (1984) or Rodriguez-Iturbe (1983).

This approach subdivides difficult problems into portions expected to be more manageable. Thus, the geometry of rainfall is subdivided into "synoptic", "large meso-scale", and "small meso-scale" areas and "cells". It is assumed that, within each of these ranges, the autocorrelation function is exponential, like a Markov process so that many standard methods of analysis become available. Unfortunately, in order to achieve the clustering that is observed in rain "events", it becomes necessary to subordinate the small-scale processes to the large-scale processes. This subordination raises profound difficulties, however, and it is widely recognized by practitioners that actual implementations are artificial. In particular, implementation involves large numbers of parameters.

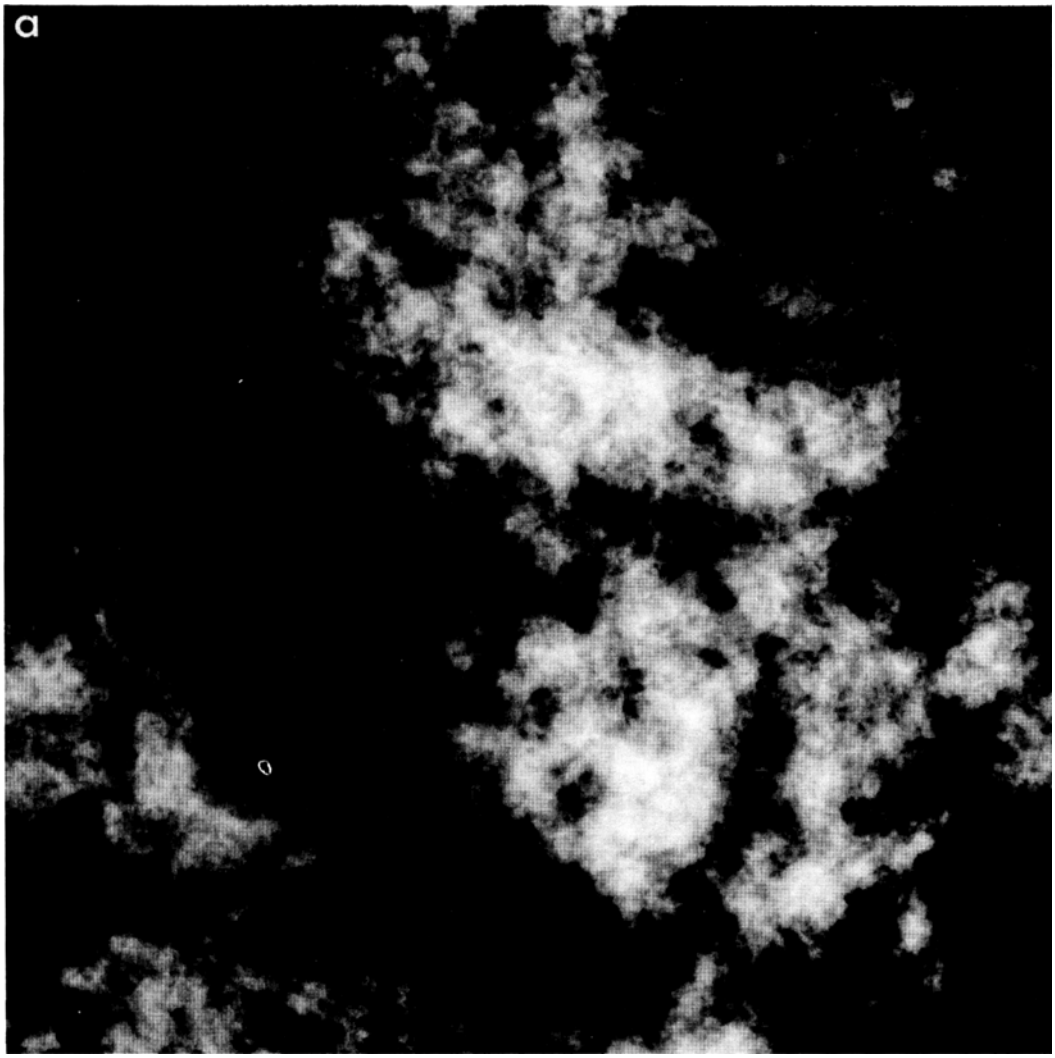

Fig. 15a. Starts a series showing parallel 800 × 800 sections of a 3-D spherical shell model, $\Lambda = 1.1$, $v = 0.33$ (density of shell centers per unit volume), $s = 2$, $\rho_0 = 2400$. These sections may be interpreted as showing the temporal evolution of a rain field when the Taylor hypothesis of "frozen turbulence" holds. (b) Same as Fig. 15a, except at a later "time" (40 pixels later). (c) Same as Fig. 15b, except at a later "time" (40 pixels later). (d) Same as Fig. 15c, except at a later "time" (40 pixels later).

They are to be determined by using rainfall data at specific time and space scales, and none of them appears to reflect in any direct fashion the basic physics of the rainfall process. Moreover, when the resulting process is used to generate synthetic storms (e.g., in hydrological modeling), the results of extrapolation are poor except for the range of scales for which the model had been calibrated.

Thus, the most persuasive argument for distinguishing several ranges of scaling in the atmosphere resides in the smallness of the scale height in the atmospheric mean pressure field (~10 km) compared with its width. Nevertheless, the vertical fluctuations do not appear to have a scale height, and (Subsection 4.3) the differences between the horizontal and vertical scaling laws can be accoun-

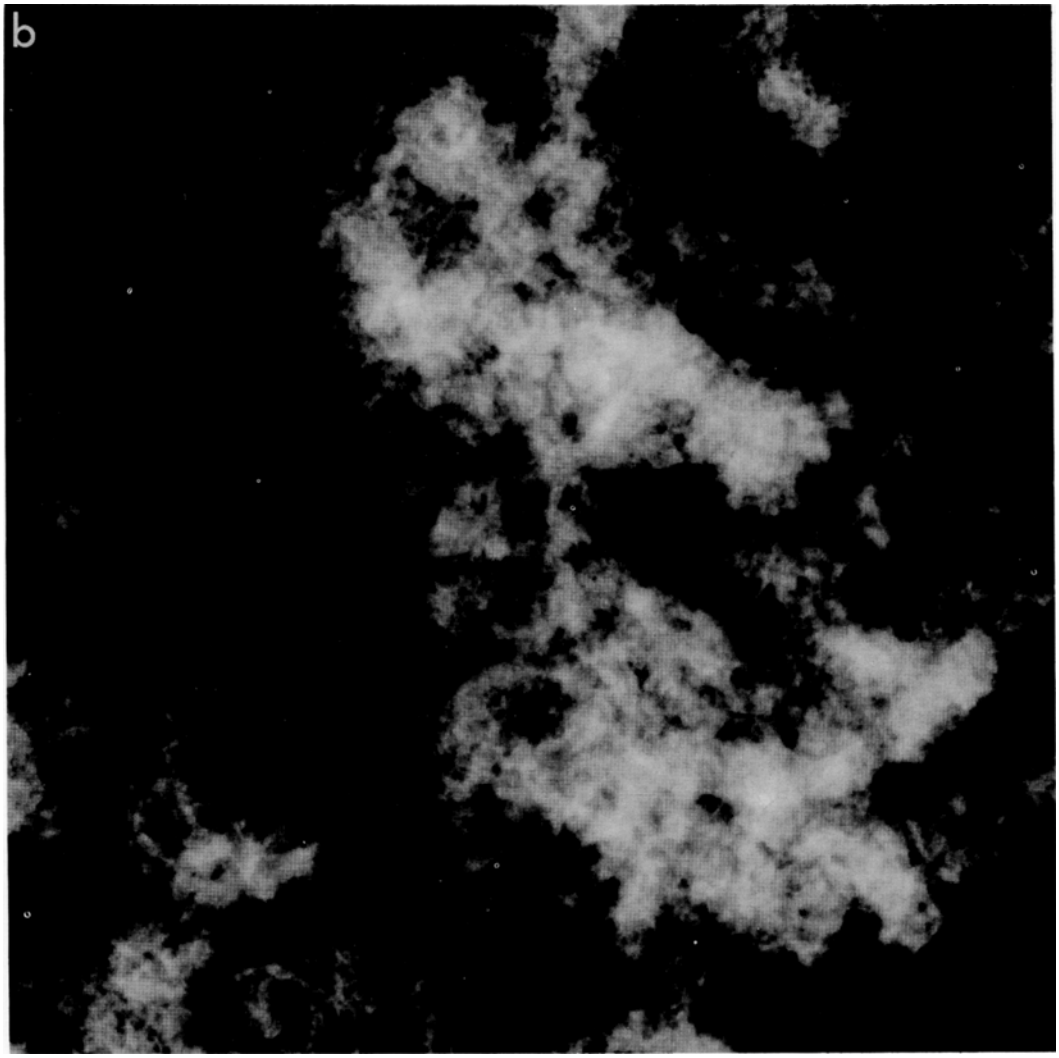

Fig. 15b.

ted in a different fashion, by an anisotropic fractal model of dimension 2.555.

To attack numerous analogous problems that occur in other areas of science, the theory of fractals forsakes subdivision. This approach had at one time seemed doomed to failure, yet it has repeatedly turned out to be successful on the following major grounds. (1) Fractals provide a successful phenomenological description of a broad class of phenomena using a very small number of parameters. (2) These parameters can be estimated consistently and with high precision, and can be related to other—more familiar—quantities of interest. (3) Furthermore, the availability of a fractal description has invariably soon triggered theoretical investigations that have justified the fractal assumptions and led to substantial overall progress.

Most relevant from the viewpoint of meteorology is turbulence, which is ruled by the same equations, those of Navier–Stokes. Since the Navier–Stokes equations involve no scale above a very small inner cutoff associated with viscosity, Mandelbrot had recourse to the so-called "principle of symmetry": when a problem is "symmetric" (that is, is invariant under a class of transformations which need not be

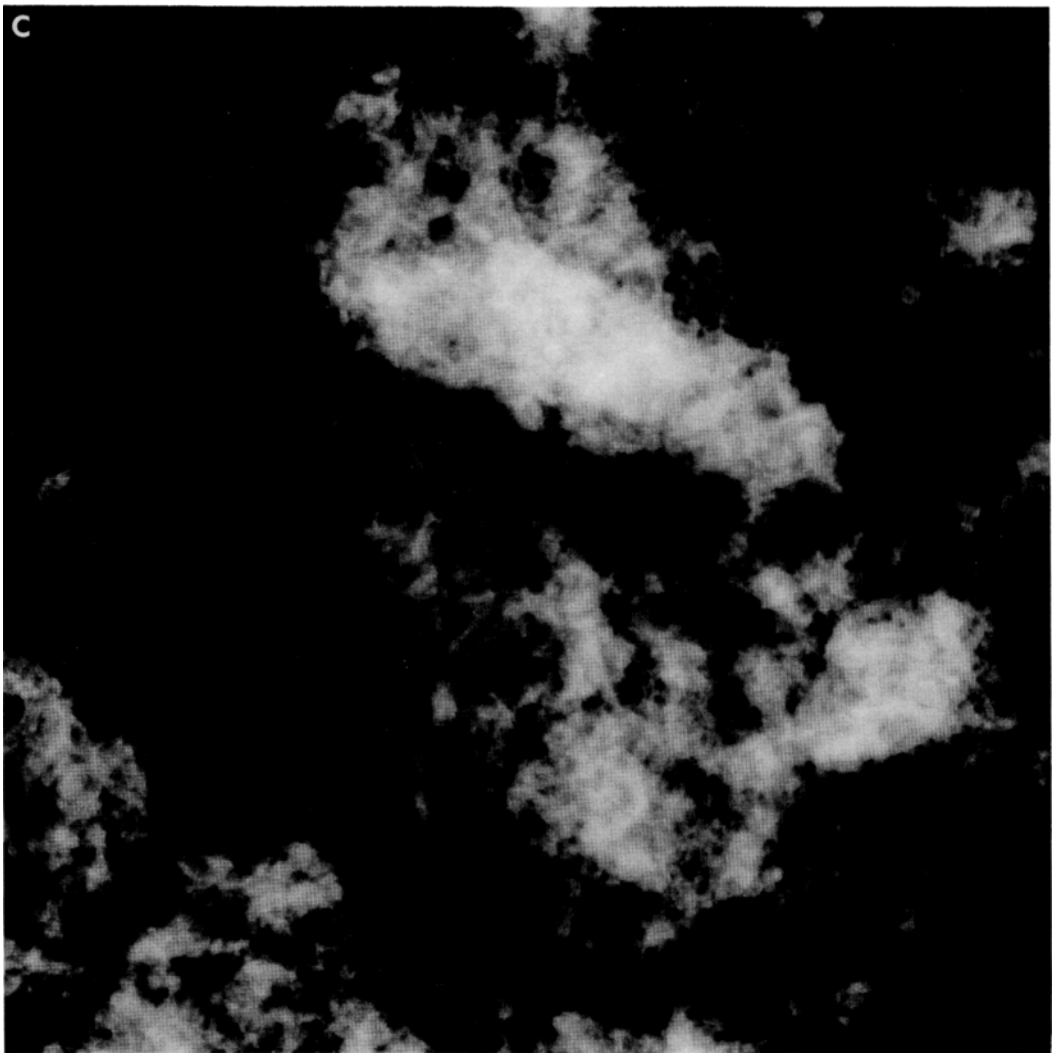

Fig. 15c.

left and right symmetry), the problem's solution should also be expected to be symmetric. Exceptions do occur, when a symmetric solution would be against other laws of nature, in which case a "symmetry breakdown" occurs. As applied to the Navier–Stokes equation, (most explicitly in Chapter 11 of Mandelbrot (1982)), this argument led Mandelbrot to the hypothesis that the phenomenon of turbulence is a reflection of scaling singularities of the Navier–Stokes equations and of their Euler limit for zero viscosity. This hypothesis has proven very fruitful, and many writers believe it is in the process of being confirmed. While skeptics may still consider that such a bold conjecture needs further confirmation, there is no question that the fractal approach has brought in a fresh perspective and new activity in the study of Navier–Stokes equations.

Our hope is that the same will be the case to some extent with the models presented in this paper. Further encouraging features reside in the fact that the boundary conditions of weather include many fractals: such as the shape of the mountains and coastlines (Mandelbrot, 1975, 1977, 1982), and atmospheric forcing (solar insolation), (private communication from C. Gauthier, 1984).

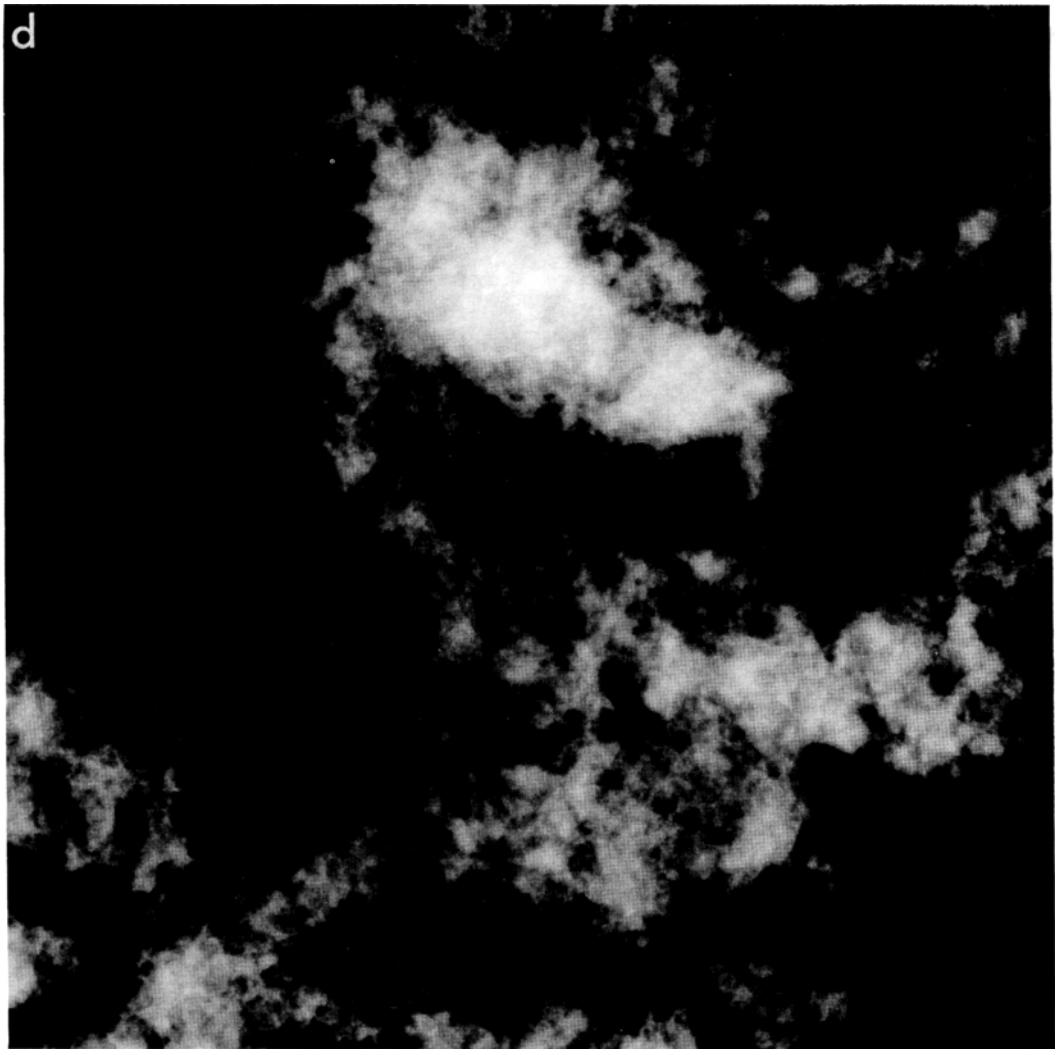

Fig. 15d.

6. Conclusions

We have proposed a fractal model for the static structure and the temporal evolution of the horizontal rain field based on three basic parameters: the scaling parameter H_E, the intermittency parameter α, and the lacunarity parameter Λ. Two other parameters—the smoothness parameter s, and the pulse density parameter ν, were also introduced but could not be determined very accurately; within a wide range, their influence seems limited to higher-order statistical properties of the model.

The scaling parameter H_E relates the large- and small-scale structure of a fractal field, and was determined from tropical radar rainfall data to have a value $H_E \sim 0.50$. The intermittency parameter α is the hyperbolic exponent of the distribution of rainfall fluctuations from isolated storms. In Montreal, in Spain, and in the tropical Atlantic, it was found to have a value $\sim\frac{5}{3}$.

In 2-D, the fractal sum of pulses model of Mandelbrot (1984c) consists of a hierarchy of annular shaped unit fluctuations. It was used to produce a scaling fractal rain model with $\alpha = \frac{5}{3}$ and $H_E = 1/\alpha$ (= 0.60). By making the annuli progressively thinner (increasing Λ) the model's struc-

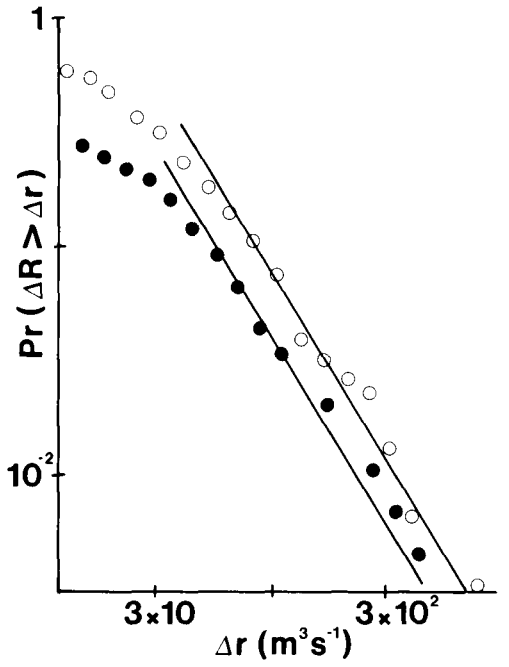

Fig. 16. A comparison of the empirical distribution of change of rainflux ΔR from isolated storms (open circles are from Fig. 3a, $\Delta t = 5$ min), and from the model with $v = 2$, $\rho_0 = 180$, $s = 2$, $\Lambda = 1.2$ on a 60×60 grid using 50 consecutive sections, $\Delta t = 1$ units apart (shown as closed circles, arbitrary units). The straight lines indicate $(\Delta r)^{-5/3}$ behavior. This shows that using smooth echoes ($s = 2$) doesn't alter the "Lagrangian" statistic α.

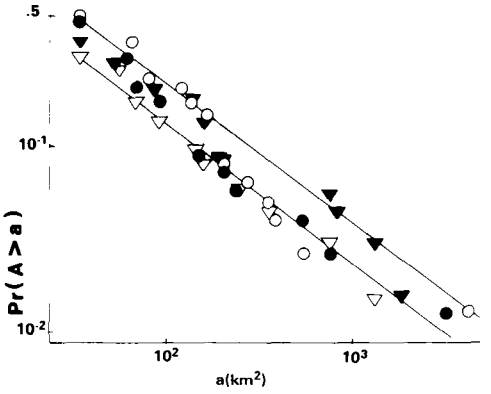

Fig. 17. The probability distribution of rain areas $\Pr(A > a)$ from four (near instantaneous) radar scans during the GATE experiment (at intervals of several hours), showing $B \sim 0.75$, from Warner and Austin (1978). The different symbols are for different scans. There were about 50 rain areas per radar scan.

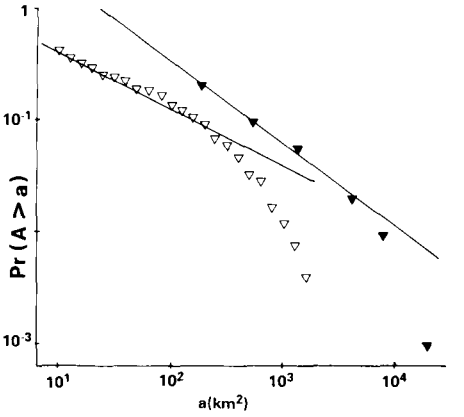

Fig. 18. A comparison of the probability distribution of rain areas $\Pr(A > a)$ for the 90 day GATE experiment (1 scan per day, 1056 rain areas, replotted from Houze and Cheng (1977)) with the model, $\Lambda = 1.1$, $s = 2$, $\rho_0 = 360$, $v = 1$ on a 120×120 grid. Model areas have been pooled over 20 successive 2-D sections at intervals of $\Delta T = 4$ units. The abscissa for the model is in (pixel)^2 not km^2. The straight lines show $a^{-0.5}$ and $a^{-0.75}$ functions respectively.

tures become increasingly banded and simultaneously more fragmented. A value $\Lambda = 1.2$ seemed visually realistic. The model is easily generalized to 3 dimensions (x, y, t) by replacing the annuli by spherical shells. The application of this model to the evolution of rain fields relies upon Taylor's hypothesis of frozen turbulence. Computer simulations showed that the model correctly simulated the hyperbolic temporal intermittency of rain flux fluctuations from isolated storms.

The model shapes had fairly realistic fractal dimension ("complexity"), and distribution of areas, although the boundaries were not quite smooth enough (D too large) and the large areas were found to be slightly too frequent compared to the small areas (B too small). The relationship between temporal and spatial fluctuations was investigated by studying the effect of pooling empirical area distributions over different time periods. To sample correctly the distribution of large areas, data must be pooled over very long periods. Further studies are required to fully understand this phenomenon.

Table 1 summarizes various model parameters and those measured by actual experiments. We believe that the agreement is good, considering the simplicity of the present fractal model. Other realistic features include the clustering of "cells"

Table 1. *Various fractal parameters estimated from the data, and the corresponding values in the simulation based upon the estimated* α *and* Λ

	α	H_E	H_L	B	D
Data	1.66 ± 0.05[2]	0.50 ± 0.02[1]	0.64 ± 0.05[2]	0.75 ± 0.05[3]	1.35[4]
Model[5]	$\frac{5}{3}$	$\frac{1}{3}$	0.72 ± 0.05[6]	0.50 ± 0.05	7/5[7]

[1] GATE data yield 0.48 ± 0.02, and Montreal data yield 0.50 ± 0.05.

[2] Putting together data for GATE, Montreal and for Spain.

[3] GATE data only.

[4] GATE and Indian Ocean data yield $D = 1.35$ (Lovejoy, 1982), data over France yield $D = 1.38$ (Lovejoy et al. 1983), and data over the Mediterranean yield $D = 1.345$ (Cahalan, private communication).

[5] The row marked "model" was obtained with $\alpha = \frac{5}{3}$, $H_E = \frac{1}{3}$, $\Lambda = 1.2$, $\nu = 1$, $s = 2$, $\rho_0/l = 3$, except where indicated under [5] or [6]. Over a considerable range, the parameters were insensitive to the values of ν and of s (e.g. $1 > \nu > 0.1$, $12 > s > 1$), and, with the exception of D, were insensitive to changes in Λ. The value of Λ does affect the lacunarity, but a quantitative investigation of this parameter is outside the scope of this paper. All of these parameters are expected to be independent of R_T—i.e., the % coverage, although this, for certain high-order statistics, may not be true.

[6] This value was estimated from the fluctuations in model rain from the evolution of 1-D connected sections with $s = \infty$ (the 1-D analog of the 2-D "Lagrangian" H_L described in Subsection 2.2). This 1-D estimate of H_L is far easier to calculate than the true 2-D value. $s = \infty$ was chosen rather than $s = 2$ because the former was hyperbolic ($\alpha = \frac{5}{3}$), while the latter was not.

[7] $D = 2 - 1/\alpha$, as described in Subsection 4.1.

and the existence of "fronts" and "bands" at all scales. The model is very flexible in that it apparently yields scaling and the correct hyperbolic temporal intermittency irrespective of the basic shape. The constraint $H = 1/\alpha$ can be lifted to allow $H < 1/\alpha$, but this requires a generalization of the FSP process, which cannot be dealt with here.

Other possibilities for extending and improving the model include modeling the vertical structure by using the notion of 'stochastic stratification" and taking the Coriolis force into account ("stochastic zonality"), as in Schertzer and Lovejoy (1984a). It will also be interesting to relate the model parameters to those of other meteorological fields. Finally, this model may prove useful in the modeling of other hyperbolically intermittent scaling fields, as Schertzer and Lovejoy (1984a, b) argue for the case of the wind, temperature, buoyancy force and energy flux fields.

7. Acknowledgements

We acknowledge many helpful discussions and comments of D. Schertzer. One of us (S.L.) thanks G. L. Austin for support and encouragement, particularly during the early stages of this project, the National Science and Engineering Research Council (Canada) for partial financial support, and the IBM T. J. Watson Research Center for its hospitality during several visits.

REFERENCES

Brown, P. S. and Robinson, G. D. 1979. The variance spectrum of tropospheric winds over Eastern Europe. *J. Atmos. Sci. 36*, 270–286.

Cahalan, R. F., Wiscombe, W, and Joseph, J. H. 1981. Fractal clouds from Landsat. NASA Greenbelt, MD, preprint.

Feller, W. 1971. *An introduction to probability theory and its applications.* Vol. II, John Wiley and Sons, New York, 567 pp.

Hentschel, H. G. E. and Procaccia, I. 1984. Relative diffusion in turbulent media: the fractal dimension of clouds. *Phys. Rev. A29* (3), 1461–1470.

Houze, R. A. and Cheng, C. 1977. Radar characteristics of Tropical Convection observed during GATE: mean

properties and trends over the summer season. *Mon. Wea. Rev. 105*, 964–980.

Hurst, H. E. 1951. Long-term storage capacity of reservoirs. *Tr. of the American Society of Civil Engineers. 116*, 770–808.

Larsen, M. F., Kelley, M. C. and Gage, K. S. 1982. Turbulence spectra in the upper troposphere and lower stratosphere at periods between 2 hours and 40 days. *J. Atmos. Sci. 39*, 929–1176.

Lopez, R. E. 1977. The lognormal distribution and cumulus cloud populations. *Mon. Wea. Rev. 105*, 865–872.

Lovejoy, S. 1981. A statistical analysis of rain areas in terms of fractals: Preprints, 20th Conf. on Radar Met., AMS, Boston, 476–484.

Lovejoy, S. 1982. The area-perimeter relation for rain and cloud areas. *Science 216*, 185–187.

Lovejoy, S. 1983. La géometrie fractale des regions de pluie et les simulations aléatoires. *Houille Blanche, 5/6*, 431–436.

Lovejoy, S., Tardieu, J. and Monceau, G. 1983. Etude d'une situation frontale; analyse météorologique et fractale. *La Météorologie VI*, 111–118.

Lovejoy, S. and Schertzer, D. 1983. Evidence of a 40,000 year scaling regime in climatological temperatures. IInd Inter. Meeting on Statistical Climatology, Lisbon, Portugal, 26–30 Sept. 1983, 16.1.1–16.1.5. Instituto Nac. de Met. e Geof., Lisbon.

Lovejoy, S. and Schertzer, D. 1984. Scale invariance in climatological temperatures and the local spectral plateau (available from the authors).

Mandelbrot, B. B. 1963a. New methods in statistical economics. *J. Pol. Econ. 71*, 421–440.

Mandelbrot, B. B. 1963b. The variation of certain speculative prices. *J. of Business* (Chicago) *36*, 394–419; reprinted in *The random character of stock market prices*, ed. P. H. Cootner, 297–337. Cambridge, MA, MIT Press.

Mandelbrot, B. B. 1965. Une classe de processus stochastiques homothétiques à soi; application à la loi climatologique de H. E. Hurst. *Comptes Rendus* (Paris) *260*, 3274–3277.

Mandelbrot, B. B. 1972. Statistical methodology for non-periodic cycles: from the covariance to R/S analysis. *Ann. Econ. Soc. Meas. 1*, 259–290.

Mandelbrot, B. B. 1974. Intermittent turbulence in self-similar cascades: divergence of high moments and dimension of the carrier. *J. Fluid. Mech. 62*, 331–358.

Mandelbrot, B. B. 1975. *Les objets fractals: forme, hasard et dimension.* Paris, Flammarion, 187 pp. A second edition appeared in 1984.

Mandelbrot, B. B. 1982. *Fractals: form, chance and dimension.* San Francisco, Freeman and Co., 365 pp.

Mandelbrot, B. B. 1982. *The fractal geometry of nature.* New York, Freeman and Co., 461 pp.

Mandelbrot, B. B. 1984a. Fractals in physics: squig clusters, diffusions, fractal measures and the unicity of fractal dimensionality. *J. Stat. Phys. 34*, 895–930.

Mandelbrot, B. B. 1984b. Fractal sums of pulses, and new random variables and functions. (Available from the author.)

Mandelbrot, B. B. and Wallis, J. R. 1968. Noah, Joseph and operational hydrology. *Wat. Resour. Res. 4*, 909–918.

Mandelbrot, B. B. and Wallis, J. R. 1969. Robustness of the rescaled range R/S in the measurement of noncyclic long run statistical dependence. *Wat. Resour. Res. 5*, 967–988.

Rodriguez-Iturbe, I. 1983. Probabilistic modeling of the precipitation process, pp. 6.1.1–6.1.7. II Inter. Meeting on Statistical Climatology, Lisbon, Portugal, Sept. 26–30. Instituto Nac. de Met. e Geof., Lisbon.

Rodriguez-Iturbe, I., Gupta, V. K. and Waymire, E. 1984. Scale considerations in the modeling of temporal rainfall. *Wat. Resour. Res. 20*, 1611–1619.

Schertzer, D. and Lovejoy, S. 1984a. The dimension and intermittency of atmospheric dynamics. In: *Turbulent Shear Flow 4*, ed. B. Launder. New York, Springer, pp. 7–33.

Schertzer, D. and Lovejoy. S. 1984b. On the dimension of atmospheric motions. In: *Turbulence and chaotic phenomena in fluids*, ed. S. Tatsumi. North-Holland, pp. 505–512.

Schertzer, D. and Lovejoy, S. 1985. Fractales anisotropes et dimensions elliptiques (available from the authors).

Tsonis, A. A. and Austin, G. L. 1981. An evaluation of extrapolation techniques for the short-term prediction of rain amounts. *Atmos.-Ocean 19*, 54–65.

Tsonis, A. A., Austin, G. L. and Lovejoy, S. 1984. A proposal for a new statistical technique for the design and evaluation of cloud seeding experiments. *Atmos.-Ocean, 22*, 67–82.

Warner, C. and Austin, G. L. 1978. Statistics of radar echoes on day 261 of GATE. *Mon. Wea. Rev. 106*, 983–994.

Waymire, E., and Gupta, V. K. 1981. The mathematical structure of rainfall representations Part 1–3, *Wat. Resour. Res. 17*, 1261–1294

Zawadzki, I. I. 1973. Statistical properties of precipitation patterns. *J. Appl. Meteorol. 12*, 459–472.